100 years of monitoring in the Swiss National Park reveals overall decreasing rock glacier velocities

Check for updates

Alberto Muñoz-Torrero Manchado [1,2 ✉], Simon Allen[1,3], Alessandro Cicoira [3], Samuel Wiesmann[4], Ruedi Haller[4] & Markus Stoffel [1,5,6]

The rock glaciers of the Swiss National Park were the first in the world where in-situ measurements of surface displacement were undertaken, starting with the pioneering work of Chaix in 1918. Our research is focused on the four rock glaciers described by Chaix, bridging the historical data gap that existed between their early 20th-century measurements and the most recent observations. Through the application of photogrammetric techniques, we geomorphologically analyze the spatiotemporal evolution of rock glaciers in the region, and disentangle the interplay with their adjacent glaciers. We show that these rock glaciers are in different phases of degradation with a general trend of deceleration and loss of volume. Our findings reveal historical kinematic changes influenced by the hydrological contributions of adjacent glaciers, which were closely connected since the Little Ice Age but are now severely degraded. The observed hydrological control, suggests that ongoing climate-induced glacier degradation will likely result in a future scenario with limited new accelerations. Instead, a steady water flow from adjacent glaciers may sustain a gradual secondary creep, progressively slowing as permafrost degradation continues, driven by predicted warming and dry climatic conditions in the Alps.

Rock glaciers (RG) are described as lobed or tongue-shaped landforms formed by a mixture of ice and frozen debris that are setting-up through gravity-driven creep[1]. They are also known to react sensitively to climate change, but summer thaw is attenuated in comparison to glaciers due to the insulation provided by the thawed active layer[2].

In October 2022, RG of the Engadin (Southeastern Swiss Alps) were included by UNESCO as one of the 'First 100 International Union of Geological Sciences (IUGS) Geological Heritage Sites'[3]. This recognition was based on the high relevance of these RG, which serve as a reference for permafrost research in the Alps and where displacement rates measured over a period extending for more than 100 years are the oldest available globally. Shortly after the creation of the Swiss National Park (SNP) in 1914, Emile and André Chaix made the first in-situ measurements of the velocity of a RG in the world[4]. During their fieldwork in 1918 and subsequent years, they assessed four RG in the SNP, the very ones we analyze in this study. Even if at that time, Chaix did not associate them as equivalent forms to those first described as RG by Capps[5] in Alaska, in later decades it was

known that they were actually equivalent[6] and thus making these RGs the first ones to be described in the European Alps. The four RGs analyzed by[4] were Val Sassa and Val da l'Acqua, where the most extensive measurements and analyses were realized, as well as Valletta and Tantermozza, which they simply visited and briefly described. Two decades later, André Chaix took new measurements again on the same boulders in Val Sassa and Val da l'Acqua[7]. However, after these pioneering measurements, for decades there have been no new velocity data registered, until the most recent annual Differential Global Navigation Satellite System (DGNSS) measurements in Val Sassa and Val da l'Acqua were initiated by the GIS group of the SNP in 2006.

So far, the longest kinematic analysis carried out on RGs reach back to 1922[8]. In their comprehensive study, Fleischer et al. integrated a stereo-photogrammetric map of 1922 with flow velocity profiles of 1938 and photogrammetric data from later decades to reconstruct the geomorphic evolution of the Innere Ölgruben rock glacier (Austria). Other long-term analyses, dating back to the late 1940s or mid-1950s (e.g[9–15].) are normally

[1]Climate Change Impacts and Risks in the Anthropocene (C-CIA), Institute for Environmental Sciences, University of Geneva, 66 Bvd Carl-Vogt, CH-1205 Geneva, Switzerland. [2]National Museum of Natural Sciences, Spanish Research Council MNCN-CSIC, C/ Serrano 115bis, 28006 Madrid, Spain. [3]Department of Geography, University of Zurich, Winterthurerstrasse 190, 8057 Zürich, Switzerland. [4]Swiss National Park, Runatsch 124, Chastè Planta-Wildenberg, CH-7530 Zernez, Switzerland. [5]Department of Earth Sciences, University of Geneva, 13 rue des Maraîchers, CH-1205 Geneva, Switzerland. [6]Department F.-A. Forel for Environmental and Aquatic Sciences, University of Geneva, 66 Bvd Carl-Vogt, CH-1205 Geneva, Switzerland. ✉e-mail: alberto.munoztorreromanchado@unige.ch

based on photogrammetric measurements from historical, vertically acquired aerial images, which can complement, or not, more recent GNSS surface measurements combined with Unmaned Aerial Vehicle (UAV) imagery[16,17], interferometric[18,19] and geophysical[20,21] analysis, or data from permafrost temperature boreholes[22–24]. From these regional to local analyses, some consensus is emerging that there has been an acceleration in the movement of rock glaciers in the Alps in recent decades, in parallel with the global increase in annual mean air temperature[14,25–27].

Theoretically, the acceleration of a RG can be due either to internal plastic deformation or basal shearing[22,28]. Internal plastic deformation can be enhanced by an increase of the permafrost temperature, causing changes in the viscosity and a reduction of the mechanical strength of the ice rich layer[27,29,30]. Meanwhile, most of the shear deformation takes place in the shear horizon, which is usually found at about 15 to 30 m depth[28], where in-situ observations and modeling studies have suggested that water supply from rainfall, snowmelt or melting of ground ice play a major role[22,31,32]. RG movement actually is a superimposition of both phenomena, on which the relative role played from each one will depend on the specific characteristics of the RG, including its geometry, structure and material rheology. Thus, for RGs where there is a limited contribution of rainwater or snowmelt on its surface, the dominant water inputs could be more related to the contributions of upstream catchment water[33]. In this case, when RGs are spatially related to the presence of adjacent glaciers melting at a rapid rate, as currently occurs in the Alps[34], this could have a major influence on the current and future RG dynamics during dry periods. Furthermore, advancing glaciers can impose an additional load on the root zone of RGs[35]. This mechanical pushing may displace pre-existing frozen sediments downstream and alter the arrangement of the existing debris accumulation, thereby influencing the overall dynamics of the rock glaciers.

The interaction between glaciers and RGs, in terms of the origin of RG ice, has been a subject of debate since the beginning of the study of these landforms. In fact, already in his 1923 work, Chaix described the observed RGs in the SNP as landforms possibly originating from the degradation of the frontal moraines of the receding upstream glaciers. Nowadays, debate still exists regarding the origin and formation of RGs, based on two theories that were initially opposed. On the one hand, there is the permafrost model[6,36] whereby the internal ice has predominantly a permafrost origin.

On the other hand, the ice-core theory suggests a predominantly glacial provenance[37–39]. These are two simplified theoretical end members, but other studies[40,41] propose that a synergy between both models is possible in areas where there is a glacial-periglacial coexistence[24,42–44]. In this regard, some works has shown geophysical evidence of a transition zone of relict glacier ice and permafrost connecting glaciers and RGs[45]. Yet, previous RG dating studies have typically recorded ages between 10,000 and 3000 years[46,47], which evidence older formation of RGs beyond the Little Ice Age (LIA). Additionally, in other studies displaying great complexity between these landform transitions, the use of multiple dating-methods combined with detailed morphological analysis has revealed glaciers overriding precedent RGs during the LIA[48], or emergence of RGs as consequence of ancient glacier retreat[49].

In the case of the four RGs in the SNP, each of them shows evidence of being spatially associated with glaciers that were already mapped on the first official topographic map of Switzerland at the end of the Little Ice Age (LIA) - the 1850 Dufour map[50]. However, these glaciers do no longer appear as glaciers in the Swiss Glacier Inventory (SGI) of 1973[51], even though bare glacier ice can still be seen at Tantermozza and Valletta. Meanwhile, for Val Sassa and Val da l'Acqua, one could hypothesize that these were currently extinct glaciers because according to satellite and historical aerial images from Swisstopo[52], there was almost no visible ice for decades. However, the extraordinarily hot summer of 2022[53] triggered openings in the debris that exposed glacial ice in both basins (Fig. 1) and confirmed the current existence of debris-covered glaciers in these two valleys as well.

The recent emergence of glacier ice, still visible in these two valleys, has motivated the present work, in which we have had the two primary aims of (i) filling, for the first time, the existing gap between the recent RGs surface velocity measurements and the ones made over a hundred years ago by Emile and André Chaix; and (ii) using this unique data series to study the historical evolution of the glaciers remaining in the adjacent areas, which we will refer hereafter as Adjacent Glaciers (AG) to investigate the possible interrelationships of these with the RGs. For both purposes, we use photogrammetric techniques with recent UAV imagery and hundreds of historical aerial images from different periods since 1946, which completely cover the catchments of the four RGs analyzed here. These are the same RGs described by Chaix in 1918: Tantermozza,

Fig. 1 | Exposed ice in Val da l'Acqua rock glacier. During the extraordinarily hot summer of 2022, several ablation and subsidence cracks occurred, exposing ice in Val da l'Acqua and Val Sassa in the Swiss National Park (Grisons, Switzerland). **a** General view of the Val da l'Acqua rock glacier obtained from the UAV survey acquired in September 2022 (depicted as a Colorized Point Cloud). At the top part, one can observe exposed ice masses shown in detail in (**b**). (picture taken by Michael Zehnder and Beat Pfund).

Valletta, Val Sassa and Val da l'Acqua (Fig. 2). Using photogrammetry, we have been able to reconstruct high-resolution orthophotos and digital surface models (DSM) for each period and each of the four RGs analyzed. Based on these outputs, we subsequently realized manual measurements of horizontal surface velocities of the RGs yielding more than 100 years of continuous surface velocities, and thereby to establish the longest RG kinematics time-series from observational measurements. In addition, we assessed volume and geometry changes, both across the RGs and the surfaces that were most probably covered by the AGs in the past. The extensions of AGs have been inferred from bare ice sighting and geomorphic observations based on historical imagery, together with the analysis of extremely negative elevation changes observed between successive DSMs. These analyses helped to detect a common decelerating trend in the velocity and ice degradation in RGs, along with an important AG degradation. The progressive retreat and over-deepening of the AGs are thus thought to have diminished their 'pushing' upon the RGs, through the formation of a dynamic discontinuity in the landform, which could no longer sustain the high displacement rates of RGs after the end of the post LIA.

Results

The four RGs show a decelerating trend in mean and maximum surface velocities since 1918 (Val Sassa and Val da l'Acqua) and 1946 (for Tantermozza and Valletta) (Figs. 3–4; Supplementary Data 1 SD1).
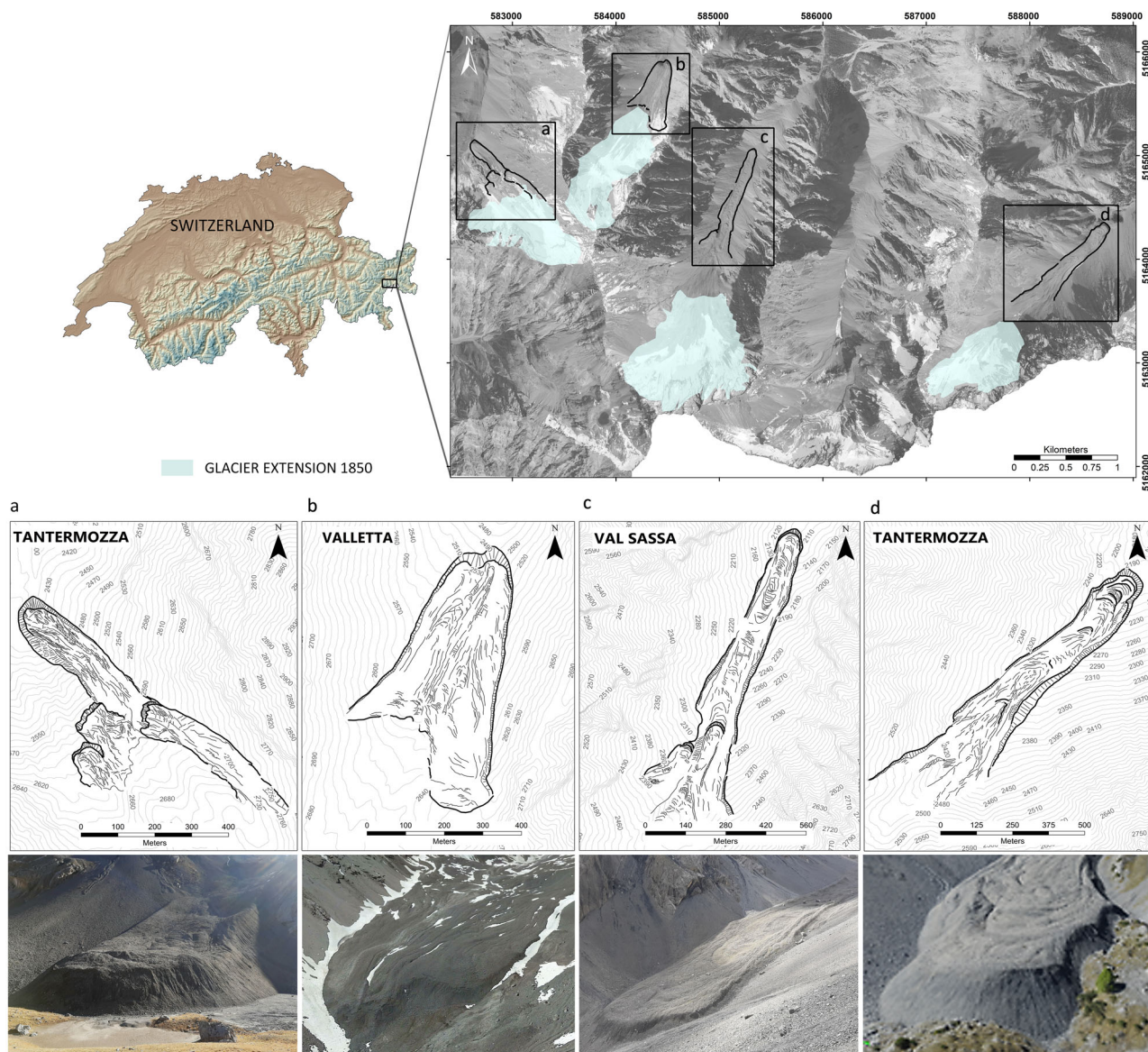

Fig. 2 | Study area. The four rock glaciers (RGs) and their catchment areas are located within a 5 km radius, entirely within the Swiss National Park (Grisons, Switzerland). All RG are tongue shaped type, creeping downwards in valleys with steep sidewalls of predominantly dolomitic lithology. **a** Tantermozza has four well-differentiated lobes, 700-m long and 300-m wide, all facing NW. With an average slope of 34%, the RG extends from 2430–2730 m a.s.l., the upper limit of the accumulation zone of the AG reaches up to 2900 m a.s.l., at a distance of 1300 m from the RG front. **b** Valletta has a single tongue facing N, it is 700 m long and 350 m at its widest area, with an average slope of 22%, at elevations between 2490 and 2660 m a.s.l. The upper limit of the accumulation zone of the AG is at 2880 m a.s.l., 1500 m away from the RG front. **c** Val Sassa is a very elongated RG facing N, with a well-differentiated main lobe in the lower zone and different minor lobes in the upper zone, it is 1180 m long and 150–200 m wide. With an average slope of 23.5%, it is found between 2110 and 2380 m a.s.l whereas the upper limit of the AG is at 2800 m a.s.l., at some 2400 m from the RG front. **d** Val da l'Acqua has a single tongue, 1170 m long by 140–220 m wide, facing NE. With an average slope of 24%, it is located between 2430 and 2730 m a.s.l. whereas the upper limit of the accumulation zone of the AG is found at 2890 m a.s.l., some 2300 m from the RG front. The study area basemap and Valletta imagery were sourced from Google Earth Pro (Image Landsat /Copernicus Image © 2024 CNES /Airbus).
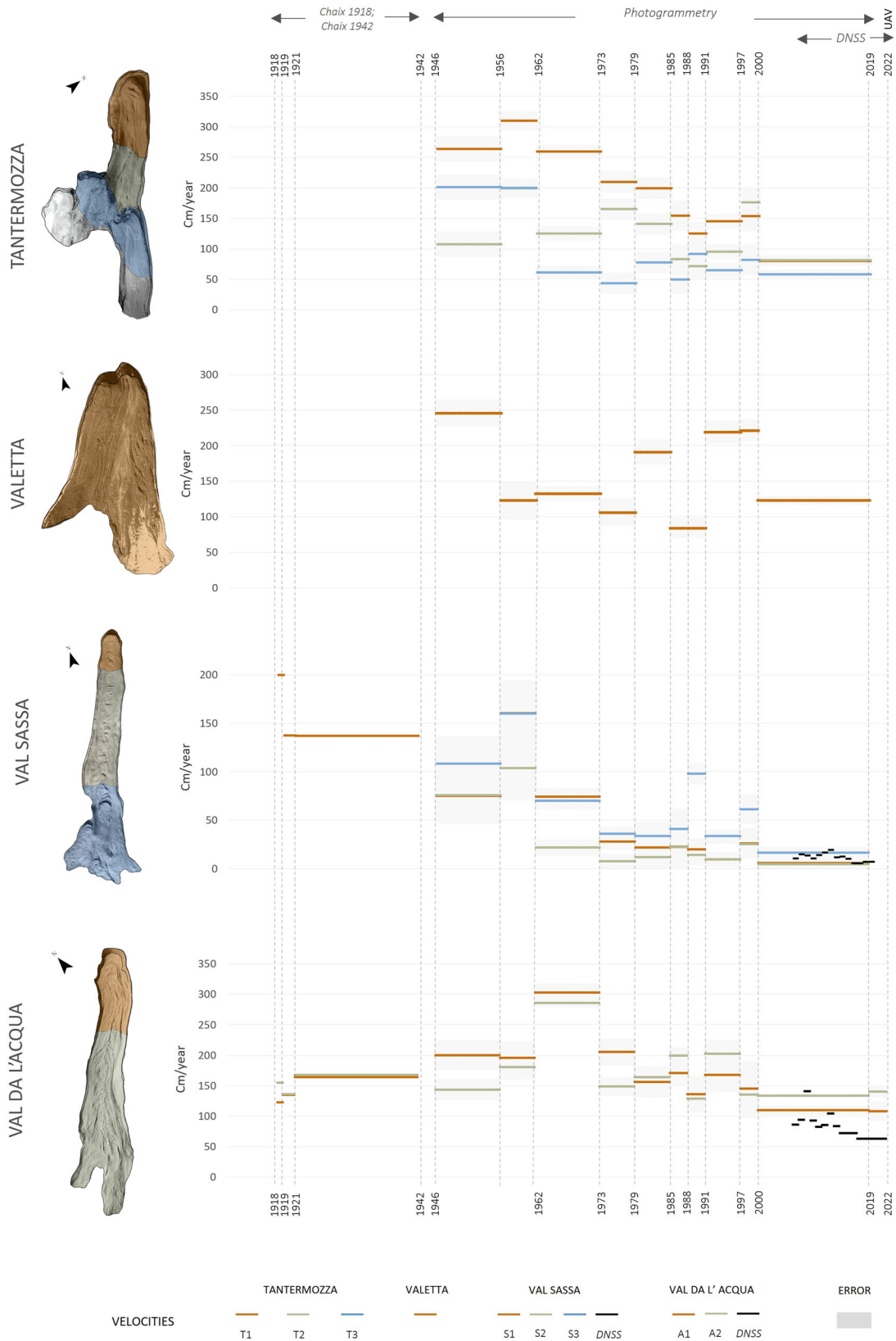
Fig. 3 | Horizontal maximum velocities. The four graphs summarize all the horizontal maximum velocities values for each of the analyzed zones of the rock glaciers from Chaix measures (1918–1942), orthophotos obtained from historical aerial imageries and UAV (1946–2022) and DGNSS measurement (2006–2022). The shaded areas correspond to the uncertainty in the measurements made on the orthophotos (see Supplementary Data 1 for raw data).
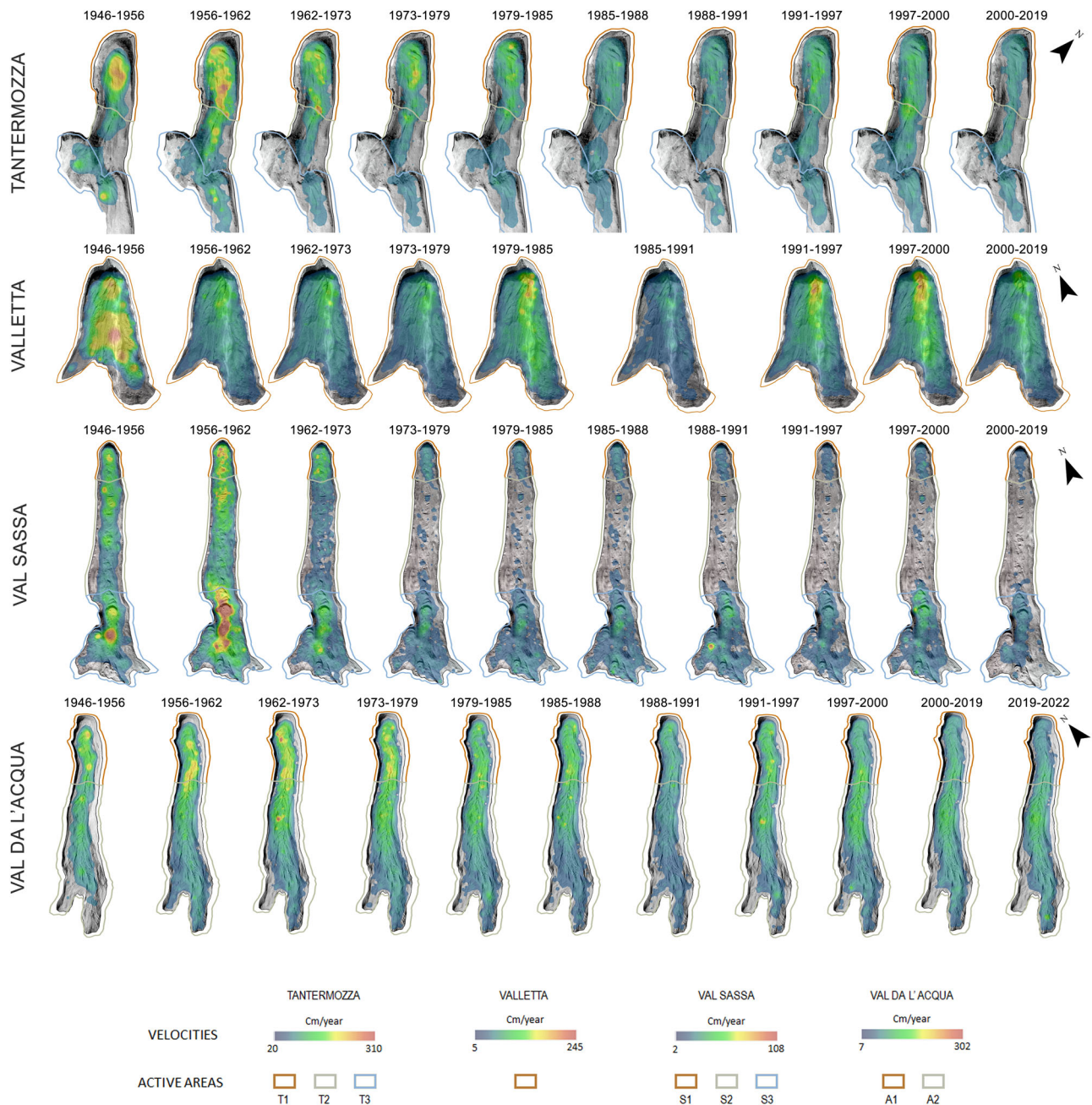
Fig. 4 | Interpolated velocity maps. The IDW interpolated maps show the spatial distribution of horizontal surface velocities (cm per year) measured in different periods between 1946–2022 within the active areas of the four rock glaciers. The active areas are separated in different zones according to different kinematics observed and shown here as different colors overlapping polygons.

Whereas some acceleration can be found in Val Sassa and Tantermozza in the 1950s, such an increase in displacement rates occurs in Val da l'Acqua in the 1960s. This temporary increase in velocities was followed by a continuous slowdown in movement rates from the 1960s and 1970s, with a common minimum at all sites between 1985/88 and 1991. After a slight acceleration in the 1990s, a steady slowdown has been observed since the turn of the 21st century, reaching record low displacement rates in recent years. This general deceleration occurs in parallel to an important volume loss at Val Sassa and Valletta (Figs. 5, 6, Table 1; Supplementary Data 1 SD1). Whereas localized elevation changes are also observed at Tantermozza and Val da l'Acqua, although there is volume loss in the upper reaches, there is aggradation in the front of the RG without loss of elevation, resulting in overall volumes today that are comparable to those of 1956. By contrast, we observe a meaningful continuous volume loss in all

the AG since 1956.. These AG show a reduction in area and retreat of the glacial fronts from positions similar to those occupied at the end of the LIA in 1850, as seen in the Dufour and Sigfried maps of 1900[50,54] (Fig. 7 and SD3), which supposedly remained in direct contact with the active areas of the RGs.

In the following, we describe the evolution of each RG in terms of surface velocities (Figs. 3, 4), volume changes (Figs. 5, 6, Table 1) as well as historical AG extensions (Fig. 7, as well as ST1 and SD1-4).

Tantermozza

Tantermozza exhibits heterogeneous kinematics across three different zones (Figs. 3, 4): The front and the middle zone of the lobe further downstream, with well-developed transversal ridges (T1); the upper zone of this lobe with longitudinal ridges in the flow direction (T2); the
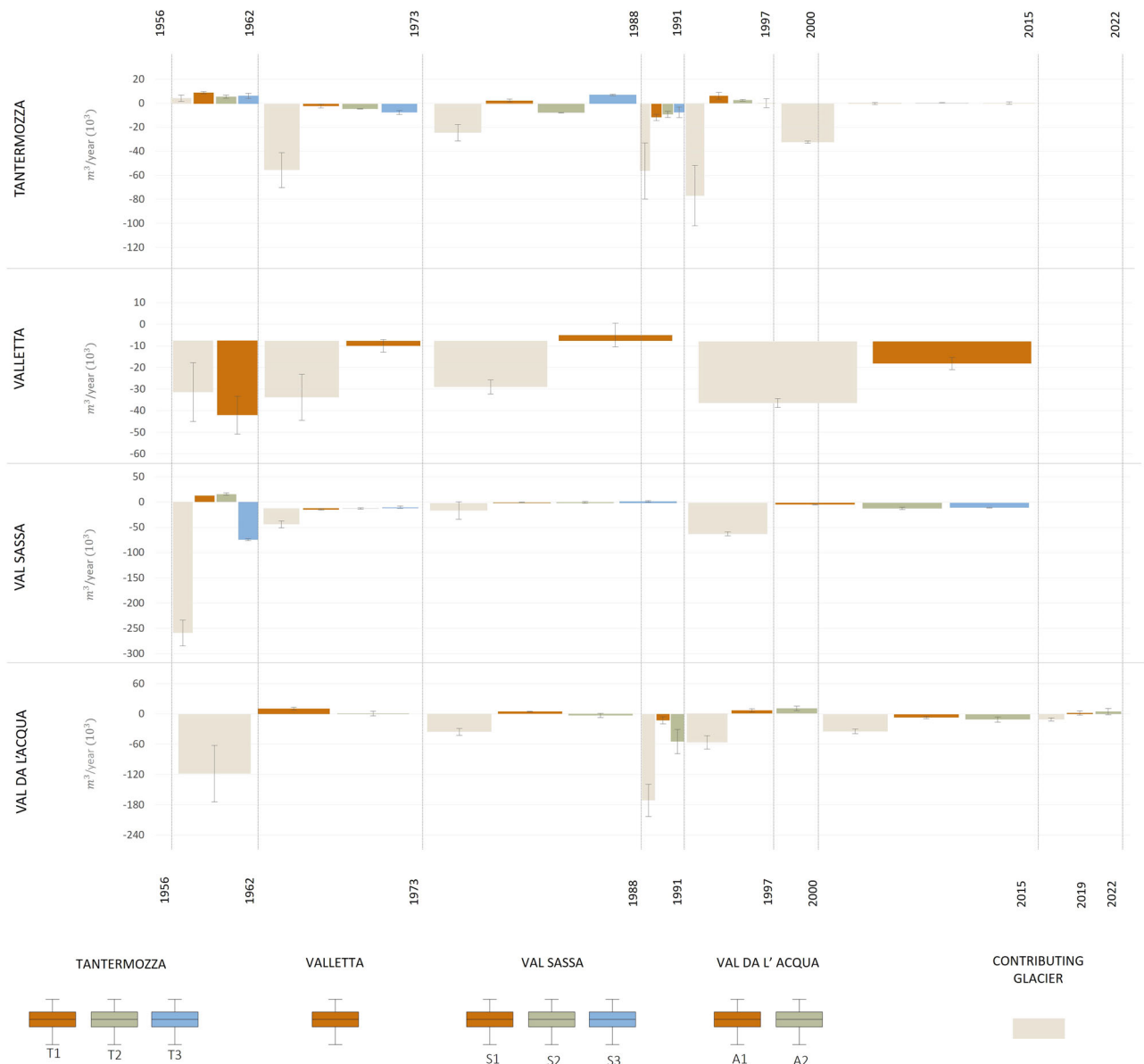
Fig. 5 | Volume change rate. Bar graphs show volume change rates in m^3 *per year* at different periods from 1956 for the different active zones of the rock glaciers and Adjacent Glaciers. Uncertainty is indicated by thin black lines.

two northernmost upper lobes (T3) with more chaotic surficial geometries, possibly caused by the AG overriding this portion of the RG during the LIA. Meanwhile, we have not observed horizontal displacements in the southernmost lobe. It presents a loss of elevation between 1956 and 2015 in these three zones, with a transition from convex shapes to a flattening in the front of T1 and with overdeepening and loss of volume of the central part in T2 and T3. Simultaneously, the AG presents a total volume loss of 2.15 (± 0.082) million m^3 between 1956–2015, which corresponds to a total loss of 16.99 m of water equivalent (m w.e.) or tons per m^2.

At the end of the LIA, the position of the glacial front occupied a location immediately in contact with the upper part of the active RG, partly overriding T3. In 1935 and until 1956, even if some glacier retreat had occurred, substantial ice bodies persisted in similar positions close to the upper lobes (T3). In an image acquired by Chaix in 1919 (SD4), as well as in the terrestrial images of 1935, we observe a marked convex transverse shape for all the active lobes of Tantermozza. During 1946–1956, maximum velocities occurred at the very front of T1, equal to 2.5 m a^{-1}, followed by 2 m a^{-1} and around 1 m a^{-1} in T3 and T2, respectively. The period

1956–1962 was the only occasion across all four catchments during which a certain volume gain is observed in the AG. A positive volume change was also observed in all active RG areas, related to the noteworthy advance of the rock glacier front and main lobes without coetaneous rise or loss in the mean elevation of the rock glacier body. During this time, T3 maintained its velocities from the previous period, whereas important accelerations are found in T2 with 2 m a^{-1}. Longitudinal ridges were formed at that time in T2 and are still present today. Meanwhile, T1 reached the highest historical velocities among all RG with 3.1 m a^{-1}. Between 1962 and 1973, a general deceleration and volume loss can be observed; it is most noteworthy in the upper zone of T3. This subsidence translates into a clear observable change in the geometry of the longitudinal and transverse profiles from convex (local heave) to flat and concave (depletion) shapes in the frontal areas of the upper lobes, along with a sharp drop in velocities from 2–0.5 m a^{-1}. These low values persist to the present day. From 1973 to 1991, a continuous deceleration is observed in the main frontal lobe where velocities decreased from 2.5–1.3 m a^{-1} in T1 and from 1.7–0.7 m a^{-1} in T2. This slowdown was mostly concentrated in an area close to the RG front, where important volume loss has occurred since 1962. This area already exhibited transversal
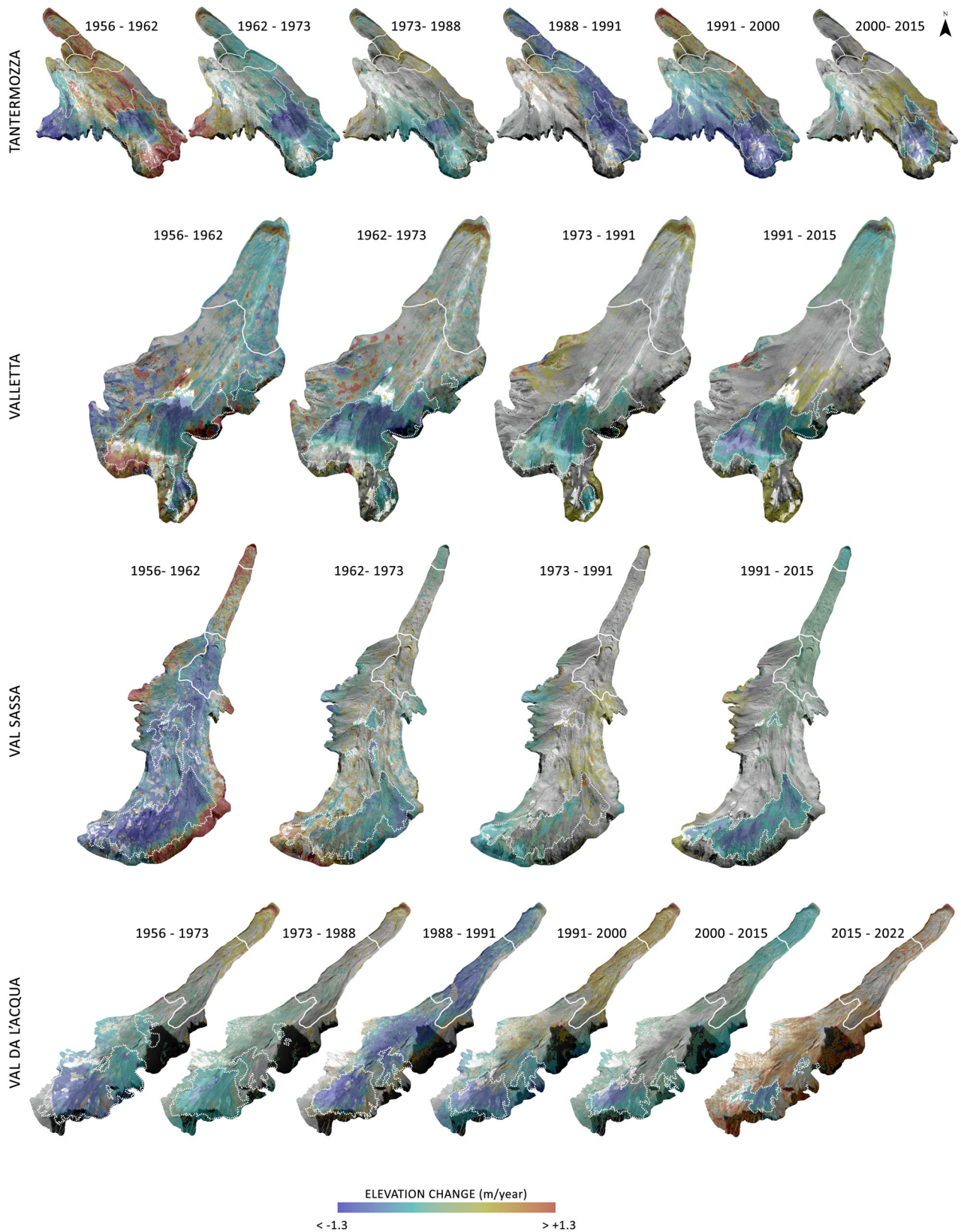
Fig. 6 | DSM differences (DSM-d) maps. These maps show total elevation changes (m) for different periods between 1956–2022 for the entire catchment areas above the forehead of the four rock glaciers, including both, rock glacier active areas (indicated by continuous white lines) and inferred glacier extensions for each period (indicated dashed white lines).

Table 1 | Total volume change

TANTERMOZZA

	GLACIER				ACTIVE RG							
	Area (m2)	Elevation Change (m/year)	Volume change (m3)	Unc. (m3)	T1 + T2 + T3 Volume change (m3)	Unc. (m3)	T1 Volume change (m3)	Unc. (m3)	T2 Volume change (m3)	Unc. (m3)	T3 Volume change (m3)	Unc.(m3)
1956–1962	126800	0.04	27734	15701	111338	16373	47214	5773	30465	7867	33659	13152
1962–1973	132800	−0.42	−608119	161205	−83406	12848	−16178	16955	−36630	2961	−30598	18629
1973–1988	109200	−0.22	−363558	102848	19760	10039	−8035	17225	21788	3561	6007	9331
1988–1991	83600	−0.67	−168455	70189	−101168	9705	−44309	7933	−34780	7830	−22080	13352
1991–1997	84400	−0.91	−460956	150372	39047	14360	50256	16897	9385	3990	−20594	22193
1997–2015	60800	−0.53	−581153	17313	8177	12494	835	15077	17663	4986	−10321	17420
TOTAL			−2154508	81942	−6251		29784		7891		−43926	

VALLETTA

	GLACIER				ACTIVE RG	
	Area (m2)	Elevation Change (m/year)	Volume change (m3)	Unc. (m3)	Volume change (m3)	Unc. (m3)
1956–1962	174400	−0.09	−162407	92771	−201285	60008
1962–1973	158000	−0.21	−530480	134702	−27404	37173
1973–1991	139200	−0.12	−439401	66797	59998	113901
1991–2015	102400	−0.17	−789424	57132	−413236	79666
TOTAL			−1921712	78167	−581927	

VAL SASSA

	GLACIER				ACTIVE RG							
	Area (m2)	Elevation Change (m/year)	Volume change (m3)	Unc. (m3)	S1 + S2 + S3 Volume change (m3)	Unc. (m3)	S1 Volume change (m3)	Unc. (m3)	S2 Volume change (m3)	Unc. (m3)	S3 Volume change (m3)	Unc. (m3)
1956–1962	312000	−0.83	−1557160	153897	−157364	10540	40139	5095	50167	13170	−247670	13357
1962–1973	229200	−0.15	−383965	82007	−14598	19116	−24935	12201	−5518	18420	15854	26726
1973–1991	196400	−0.08	−267649	311206	95218	22894	17388	11681	23169	31901	54661	25101
1991–2015	191200	−0.32	−1484372	100942	−525147	29398	−74743	18623	−237869	54587	−212536	14984
TOTAL			−3693146	166945	−601891		−42151		−170050		−389691	

VAL DA L' ACQUA

	GLACIER				ACTIVE RG					
	Area (m2)	Elevation Change (m/year)	Volume change (m3)	Unc. (m3)	A1 + A2 Volume change (m3)	Unc. (m3)	A1 Volume change (m3)	Unc. (m3)	A2 Volume change (m3)	Unc. (m3)
1956–1973	262800	−0.45	−2006638	952390	138595	57155	130086	39392	8510	74918
1973–1988	194400	−0.18	−536980	103552	12133	35505	61775	10702	−49642	60308
1988–1991	152400	−1.12	−512348	94929	−249098	46715	−46385	21370	−202713	72061
1991–2000	120800	−0.47	−512348	119968	234900	33942	90801	26561	144100	41323
2000–2015	108000	−0.31	−506495	66615	−439819	53761	−168916	30465	−270903	77057
2015–2022	43600	−0.25	−76751	22721	215482	36538	66942	28123	148540	44953
TOTAL			−4151559	307071	-87807		134303		−222109	

Total volume changes calculated from DSM of Difference (DSM-d maps) in the different zones of the active area of the rock glaciers and in the inferred areas of the Adjacent Glaciers, at different periods from 1956. Additionally, it shows area and elevation change at the inferred Adjacent Glacier area for the same periods.

ridges in the pictures taken by Chaix in 1919 and is easily recognizable nowadays with the naked eye, but also through the strong change in curvature along the longitudinal profile. Between 1988 and 1991, the largest volume losses occurred in T1 and T2; they went hand in hand with marked decelerations in movement velocities. Starting in 1991, strong ablation occurs from the AG: whereas velocities at T3 remained constant with 0.6 m a^{-1}, resulting in a practically invariable volume, T1 and T2 exhibit variations both in speeds and volumes. During the 1990s, both zones experienced accelerations and volume gains, with identical maximum speeds in both areas since 1997. Over the last two decades, T1 and T2 showed a similar deceleration, with displacement rates settling at about 0.8 m a^{-1}, without considerable volume change.
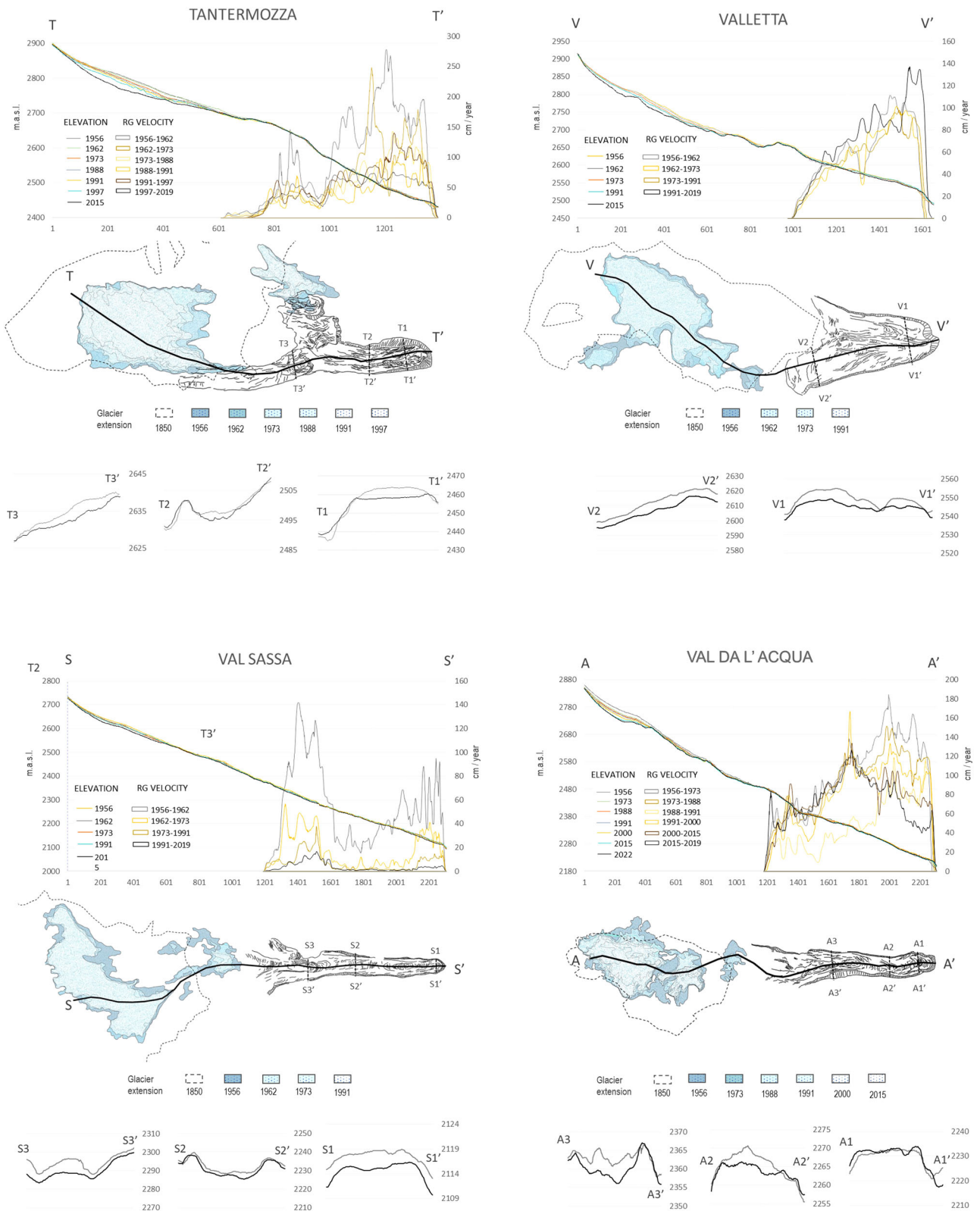
Fig. 7 | Velocity and elevation longitudinal-transverse profiles. Historical evolution of elevation changes (from photogrammetry DSMs) and measured horizontal surface velocities in the rock glaciers (RGs) for corresponding periods. Longitudinal and transverse profiles covering the Adjacent Glacier areas and the active rock glaciers are indicated by black lines at the bottom maps of each rock glacier. Boundary area of 1850 corresponds here to the Siegfried maps of 1900, which better represent in these catchments the Adjacent Glacier extensions of the Dufour map of 1850 (See Supplementary Data 4).

Valletta

Valletta presents a rather homogeneous dynamics longitudinally, with higher velocities in its eastern half. This part exhibits a continuous and homogenous flow as a single body, reflected in a characteristic morphometry of continuous longitudinal ridges and furrows, whereas transversal ridges are almost missing completely. The RG presents a total negative volume loss of 0.58 (+ − 0.081) million m³, a general loss of elevation and flattening between 1956 and 2015, whereas its AG exhibited a loss of 1.92 (+ − 0.078) million m³ (11.01 m.w.e).

In 1850, the position of the AG end moraine delimited quite closely the current upper limit of the active area of the RG. By 1935, the glacial front had already retreated approximately 300 m in the westernmost area and about 150 m in the eastern part according to terrestrial images. This differentiated retreat was maintained in the following two decades, with the easternmost part retreating another 200 m until 1956, whereas the eastern half remained in similar positions but with ice bodies becoming increasingly isolated from the main ice mass. Between 1946 and 1956, Valletta exhibits its highest historical velocities, with maxima of 2.5 m a⁻¹, like at Tantermozza at the same time. However, between 1956 and 1962, Valletta shows a completely opposite behavior to its neighbor with a drop of maximum velocities to ≤1.2 m a⁻¹, along with an important volume loss in the eastern part. In turn, contrary to what happened to the Tantermozza AG, the Valletta AG lost volume at an almost constant rate (~30,000 m³ a⁻¹) ever since that period. RG velocities and volume remained constant over the next two decades, to be followed by an acceleration in velocities between 1979 and 1985. From then on, it presents variations in surface velocities that are very similar to those of Tantermozza. A clear drop in velocity is recorded between 1985 and 1991, reaching their historical lowest values (≤1 m a⁻¹), followed by a new acceleration between 1991–2000 (~2.2 m a⁻¹) and another drop in velocities to 1.2 m a⁻¹ from 2000 to 2019. This reduction in velocities was accompanied by a general volume loss across the entire RG, with a slight flattening of the surface in the longitudinal and transverse directions. Despite this flattening, the overall shape of the RG remains more convex than at the other RGs. In the adjacent zones, the constant elevation loss is concentrated around the AG increasingly exhibiting the marked concave shape of the underlying bedrock.

Val Sassa

Val Sassa has suffered the largest drop in speeds and sudden volume loss of the four RGs. Changes are not equally intense across the RG, three zones can rather be identified with specific behavior: The front of the main lobe (S1) is characterized by transversal ridges and furrows, separated from an intermediate zone (S2) with surficial signs of thinning and subsidence; this zone is followed by the lobes of the upper zone (S3). Val Sassa RG presents a total negative volume loss of 0.60 (+ −0.023) million m³ since 1956, mostly centred around S2 and S3, whereas the AG presents a total volume loss of 3.69 (+ −0.166) million m³ (11.83 m. w.e).

On the 1850 Dufour map, the position of the AG front was barely 100 m away from the root zone of the Val Sassa RG. In the hiatus zone, stacked linear ridges can be identified in the 1935 oblique images, which we interpret as being push moraines; these ridges bounded the upper limit of the RG. Val Sassa showed the largest historical velocities with 2 m a⁻¹ in S1 during the first measurements of 1918–19. A slight decrease in speeds was already documented between 1919 and 1921 (1.4 m a⁻¹). Terrestrial images acquired by Chaix in 1918, as well as oblique images from 1935 show transverse convex shapes in S1 and S3, but also first signs of depletion in S2. Velocities remained mostly unchanged in S1 and S3 until 1942. Between 1946 and 1956, we observe a deceleration, more marked in the lower (0.7 m a⁻¹ in S1 and S2) as compared to the upper (1.1 m a⁻¹ in S3) zones. Between 1956 and 1962, movement rates increased again to ≤1.6 m a⁻¹ in S1 and S3 and to 1 m a⁻¹ in S2. This acceleration is contemporaneous to the largest volume loss of the AG with 260,000 m³ a⁻¹ as well as the largest volume loss in the active area of the four RGs with 75,000 m³ a⁻¹ in S3. These losses also resulted in a clear general flattening of the previously convex landforms. During this same period, some aggradation occurred in zones S1

and S2. By this time, the area of the AG was clearly reduced compared to 1850, but an important body of isolated ice persisted in locations that were still in contact with the upper part of the RG. Looking at the longitudinal profile, the upper parts of the AG already presented a general concave shape in 1956 which was even exacerbated after this great volume loss. From 1962 to 1973, Val Sassa RG velocities reduced in S1 and S3 down to 0.7 m a⁻¹ (i.e. to a third of previous values), with an even more dramatic drop in S2 where movement dropped to 0.2 m a⁻¹ (or one-fifth of previous value). From 1962 to 1991, volume losses did not continue at the same rate in the AG and some equilibrium can be observed in terms of volume at the RG. Noteworthy, this period of reduced losses is contemporary with the deposition of debris on previously exposed ice. The debris cover is more obvious in the eastern half of the AG and continued to build, thereby covering glacier ice completely by 2000.

After 1973, velocities in S1 and S3 dropped to 0.3 m a⁻¹, whereas S2 barely shows any movement above 0.1 m a⁻¹. Velocities remained generally low with just some acceleration in the 1990s, as at the other RGs. Since the turn of the 21st century, DGNSS and photogrammetric measurements show a decelerating trend with current velocities at S1 and S2 below 5 cm a⁻¹, and 7 cm a⁻¹ in S3. This deceleration coincided with an appreciable loss of volume at the AG (60,000 m³ a⁻¹) and substantial volume losses in all RG zones, producing, even at its front of S1, a depleted central area with respect to the margins.

Val da l'Acqua

Val da l'Acqua presents the most constant horizontal velocities of the four RGs, but suffered from a negative trend in surface velocities and important periods of volume losses too. The active areas of the rock glacier can be divided into two halves with different dynamic behavior. A lower half - close to the front (A1) and an upper half (A2). Compared to 1956, the RG now has a degraded upper part (A2) where losses total 0.22 (+ − 0.064) million m³and an aggrading front with a volume gain of 0.13 (+ − 0.027) million m³. The total volume loss of the AG amounts to 4.15 (+ − 0.307) million m³ (15.80 m w.e.), representing the greatest volume loss among the four catchments.

As in Val Sassa, the position of the AG end moraine was just slightly more than 100 m away from the active part of Val da l'Acqua RG in 1850. The glacial front can not be discerned on the historical photographs of 1918 and 1935, but according to our inferred area of the AG in 1956, the glacier ice had receded by c. 250 m with respect to the end of the LIA, leaving isolated ice patches behind. Horizontal velocities remained quite stable both in A1 and A2 from 1918 to 1962, with values ranging between 1.5 and 2 m a⁻¹, and only a slight slowdown during the period 1919-1921 (again as in Val Sassa). Between 1962 and 1973, a marked increment of the maximum speeds can be observed in very localized areas of A1 and A2 (up to 3 m a⁻¹) along with an important retreat and volume loss of the AG. Yet, these local changes in movements only had a minimal effect on the overall mean RG velocities. Between 1962 and 1973, a remarkable hiding of exposed ice can be observed, predominantly with debris, covering the easternmost area. Coverage here is less extensive compared to Val Sassa, still leaving a large area of ice exposed in the western half of the RG. It is in this western zone where the volume loss mainly occurred in subsequent decades. Glacier ablation was notable during 1988–1991, with appreciable deceleration and volume losses in A1, but even more so in A2 (60,000 m³ a⁻¹) where losses were accompanied by a more evident deceleration in velocities. Again during 1991–2000, as in the other three RGs, an acceleration is discernible in both zones, but with a gradual migration of maximum speeds from lower to more elevated zones, resulting in the highest mean velocities seen in A2. As shown by DGNSS measures, A1 is in a clear downward trend in movement since 2000, and the speed has nowadays decreased to 0.5 m a⁻¹ or less, with some localized subsidence in the upper part evident in both the longitudinal and transverse profiles. Meanwhile, velocities in A2 maintained higher values of around 1.4 m a⁻¹, with considerable depletion produced during this period. On the AG, volume loss rates have been lower than during previous decades, as the debris has come to hide the ice in its entirety. Despite this, glacier area was

reduced by almost half between 2000 and 2015 and the longitudinal profile has become closer and closer in recent years to the concave and more irregular shape of an underlying carved bedrock.

Discussion

The general decelerations and total volume loss that have occurred at different rates over the past 100 years in the four RGs of the SNP show a behavior that is consistent with RGs slowly transitioning from secondary creep towards a state of degradation[28]. This involves a transition from a steady creep rate, through a state of decreasing but still relatively high velocities due to a concurrent permafrost degradation, to a degradation state where preceding decades of permafrost thawing result in decreased driving stress and increased packing density of the RGs. This degradation is evident in the general curvature of both longitudinal and transverse profiles, indicating signs of ice depletion across all the RGs. This ice depletion is more pronounced in Val Sassa and Tantermozza, where following creep deceleration has been particularly substantial. Meanwhile, aggradation convex shapes are still present at the fronts of the Val da l'Acqua and Valletta RGs, but with a continuous flattening trend. The observed deceleration, primarily concentrated in the lower frontal regions of the main tongues, contrast with the gradual accelerations seen in the lower sections of RGs which are in a process of destabilization, such as at the Äußeres Hochebenkar[15]. This frontal deceleration is more clearly ongoing in Val Sassa and Val da l'Acqua between an elevation range of 2100 to 2300 m a.s.l. Such an elevation range is exceptionally low when compared to the lower limit of active RGs reported in extensive inventories in the Alps[26,55–57] and roughly coincides with the current lower limit of discontinuous permafrost in this area[58]. The recent more prominent deceleration at the front of the RG than in the upper parts, may be linked to a gradual upslope permafrost degradation in precedent decades, leading to the localized loss of the ice-rich layer, particularly at lower elevations. As observed in SD10, rising annual mean air temperatures (AMAT) in our study area have led to discernible negative anomalies in snow cover since the mid-1980s. This phenomenon prompts a reduction in snow cover insulation[59], which may increase annual mean ground temperatures (AMGT)[60]. When coupled with an altitudinal temperature gradient of $-0.65\,°C/100\,m$[61], this scenario provides a plausible explanation for the observed upslope shift in velocities, with AMGT above zero gradually advancing upslope in recent decades. This effect may be compounded with a progressive dynamical disconnection of the RG's fronts from the upper rooting zones. Notably, this trend is conspicuous in Val Sassa, where an elongated nearly immobile transition zone in S2 has persisted for decades. The tendencies and longer term evolution of these RGs could serve as prime examples of how RG downwasting could.

Uncertainties of historical data

Despite the distinctive nature of the records presented herein, we are well aware of several uncertainties that are inherent to interpretations related to different types of data sources with different resolutions. The uncertainties that require further assumptions likely pertain to the direct measurements by Chaix between 1918 and 1942. Although their work elucidates the detailed measurement methodology, it omits specific information on associated uncertainties or the instruments used. Despite this, as detailed in SM9, assuming typical precision levels of topographic instruments from that era allows for a rough estimation of a maximum error of around 20 cm. This is deemed acceptable, given the displacement measurements ranging from $0.8–2\,m\,a^{-1}$ during that period. Meanwhile, the uncertainty related to displacements and volume differences derived from later scanned images and UAV photogrammetry mainly depends on the quality of the images co-registration, which, in turn, hinges on image resolution. The calculated uncertainties, as evident in SD8 for horizontal displacement and vertical changes, exhibit important variability across years and sites. Nonetheless, these uncertainties set limits of detection (LoD) between $5–25\,cm\,a^{-1}$ for horizontal displacements and generally below 20 cm/year for vertical changes in AGs and RGs. We consider these values acceptable in light of the overall substantial changes observed. In addition, there are important

limitations related to the unavailability of subsurface data. This is especially the case for the volume changes, and the implications that the latter may have on RG behavior. While in the AG areas, the volume decrease would mainly be due to the ice melting, this is certainly more complex in the RGs. As RGs are composed of a mix of ice, sediments and air, if sediments are supersaturated we will see a volume change signal until debris porosity is reached, at which point a volume decrease will no longer be evident[62]. As a result, in conditions of permafrost degradation, the higher the ice content in the RG, the higher the expected volume loss. By contrast, in RGs with high content in coarse sediments, this change can be almost negligible. Besides, for active RGs, such effects have to be combined with elevation changes due to lateral extensions/compressions which can sum to produce considerable uncertainties to the calculation of ice melting volumes in RGs[11]. Despite these uncertainties, and without any pretension in this work to associate volume loss purely to ice loss in the RG, we are confident that the historical elevation changes observed, both in the longitudinal and transversal profiles of the four RGs, are of a sufficient magnitude and widespread enough, that they can be clearly associated with permafrost degradation.

Potential mechanisms of displacement

A general accelerating trend, observed in many RGs over the last decades in the Alps and in some cases triggering destabilization, has been related to an increase in atmospheric temperature and warming of permafrost causing a thermally induced accelerated creep[14,26]. Whereas certain accelerations were observed at our sites during the 1950-1960s and 1990s, there has been a general trend for a deceleration in the 20th century, consistent with a general increase in air temperatures[63,64], which could suggest that in these cases, changes in RG kinematics would be governed by (an)other factor(s) prevailing over the thermally induced plastic deformation. The historical surface kinematics observed throughout the century-long timeseries should be explained by other elements, either topographic or hydrological[24,28,30,32]. In our case, it is suggested that the spatial interaction with the AGs could have had implications regarding both factors.

On the one hand, we see that the highest recorded velocities coincide with the post LIA period during which the AG termini were almost delimiting the upper contact of the active zones of the RGs. Until the end of LIA, the stress propagation of the AGs would have been greater towards the proglacial foreland, thus promoting RG movement[35,65]. However, in the subsequent decades, as glaciers retreated, the diminishing stress resulted in a reduction in mechanical influence over the RGs.

On the other hand, changes in rock RG velocities appear to be influenced by the hydrological contribution of the AG, as long as the RG are not suffering noteworthy ice-depletion. We observe that during periods characterized by anomalously high volume-loss ratios in the AGs, but without simultaneous substantial ice-depletion in the RGs, accelerations were observed. Examples include the accelerations documented in Val Sassa and Val da l'Acqua RGs during 1956 to 1973 and those recorded in Valetta, Val Sassa, and Tantermozza RGs during the 1990s. Conversely, during periods without a notable loss of volume in the RGs but with a reduction in the hydrological contribution from the AGs compared to the preceding period, substantial decelerations occurred in the RGs. Instances include observations in Val Sassa during 1962 to 1988, in Val da l'Acqua during 1973–1988 and 2000–2022, and Tantermozza between 1973 to 1988 and 2000 to 2019. Meanwhile, in periods marked by substantial ice-depletion in the RGs, a simultaneous deceleration occurred, even in the presence of a high water supply from adjacent glaciers. This phenomenon was observed in Tantermozza between 1962–1973 and across all the RGs by the end of the 1980s. The exceptional rate of ice loss, both in the AGs and all RGs between 1985-1991 coincides with the abrupt winter warming and reduction in snow days in the Alps since the late 1980s[66] and aligned with climatic conditions in our area (SD10). This suggests a noteworthy short-response and high sensitivity of these RGs to external climatic forcing, but without an associated immediate thermal-induced creep by plastic deformation. Still, the permafrost degradation during this warming period, could have had a delaying effect promoting the general creep acceleration observed during the 1990's,

consistent with the general acceleration observed by[14] in RGs in the Western Alps during the same time-frame.

Direct observations and rheological modeling studies have shown that heightened liquid water intrusions into RG bodies can exert a short-term influence on its rheology causing thermal advection and increasing pore-water pressure[67]. Meanwhile, long-lasting changes in ice-water proportion within the RG may have implications for long-term horizontal depth flow changes[27,44]. In the event of these conditions, our observation of AG extensions and longitudinal profiles that show glaciers in a state of continuous depletion in the last decades, and with the glacier snouts increasingly further away from the active area of the RGs, would indicate a near future scenario with a complete absence of new important RG accelerations. These conditions could persist for a several more years, with the rate of melting for the nearly exhausted glaciers damped by the debris cover, as observed in Val Sassa and Val da l'Acqua. Whereas, the reduction in the cryosphere due to the transition to non-glacial conditions might lead to an increase in precipitation which is not converted to ice in the glacier. Consequently, this could result in a rise of the amount of immediate water supply into the rock glaciers (RG) from precipitation in the contributing areas, potentially intensifying basal shearing during periods with high solid or liquid precipitation. This effect might have been mitigated in the last decades by the observed positive trend in warmer temperatures and dry conditions (SD10). Consequently, a slower but continuous flow of water from the AGs would thus maintain a slow secondary creep that would continue to gradually slow down as the permafrost is slowly degraded.

Spatial interrelationships between glaciers and rock glaciers

Regarding our observations of the historical spatial interrelationships between AGs and RGs, we cannot draw solid conclusions about the origin of the rooting ice of the four RGs beyond the observed proximity between them at the end of the LIA in 1850. Even so, the observed signs of glacial overriding on the surface of the upper lobes at Tantermozza RG, and the small push moraines just above the top part of the RG of Val Sassa, could correspond to the maximum limit of the glacier advance at the end of LIA. We infer that these cases are similar to the interactions between the glacier of Vadret Muragl and the RG of Muragl[48], situated just 5 km north-west of our study area, on which the RG was precedent to the overriding glacier. But more importantly, that the morphology and main lobes of the four RGs already presented an extensive development and positions similar to the current ones in 1918. As occurs in the RG of Muragl, it is thus very unlikely that the current RGs frontal lobes were formed from end glacial ice after the end of the LIA, which would suggest retreat distances between 700–800 m for Valetta and Tantermozza and 1000–1200 m for Val Sassa and Val da l'Acqua between the year 1850 and 1918. Despite this, we cannot exclude that much older glacier retreats were involved in the origin of the debris material forming the RGs, as was demonstrated in the Héðinsdalsjökull RG in Iceland[49]. While, conducting geophysical surveys or borehole investigations in these former contact areas could certainly help to decipher the former and current AG-RG interrelationship, such investigations will not be possible in the strictly protected environment of the Swiss National Park.

Methods
Antecedent works
Émile and André Chaix undertook the first in-situ measurements between 1918–1919 and 1919-1921 for Val Sassa and Val da l'Acqua RGs[4]. During their different field campaigns, they acquire relative displacement measurements carried out on boulders that were along transversal profiles, located both near the front of the RG as well as in the upper areas (SD9). Two decades later, in 1942, André Chaix revisited the sites and took new measurements on the same boulders[7]. Unfortunately to date, efforts to locate these boulders again have not been successful, and therefore, it has not been possible to continue tracking movements using the same elements. The next known measurements were made by Heinrich Jäckli in Val da l'Acqua[68]. In this work he summarized past measurements for Val da l'Acqua forehead (1921-1942-1968) and acquired new velocities between 1968–1979. These

measurements were conducted using different boulders than the ones measured by Chaix, but again, in the current study we have not been able to find their exact location. Even so, they serve as a reference to compare against our photogrammetric measurements from the same period.

For the last 2 decades, Differential Global Navigation Satellite System (DGNSS) surface measurements have been systematically acquired (almost yearly) by the GIS group of the SNP using boulders at 8 different positions along the Val Sassa RG body (years 2006,2007, 2008, 2009, 2010, 2011, 2012, 2013, 2014, 2015, 2016, 2018, 2020) and 19 locations near of the front of Val da l'Acqua (years 2007, 2008, 2009, 2010, 2011, 2012, 2013, 2014, 2015, 2017, 2022). See SD5 for the locations of the DGNSS measurements.

Photogrammetry
With the aim of filling the gap between the older measurements from Chaix (1918–1942) and the recent ones from DGNSS (2006–2022) in Val Sassa and Val da l'Acqua, and to obtain the first measurements for Tantermozza and Valletta RGs, we created orthophotos and DSM by carrying out photogrammetry processing from historical imagery and UAV.
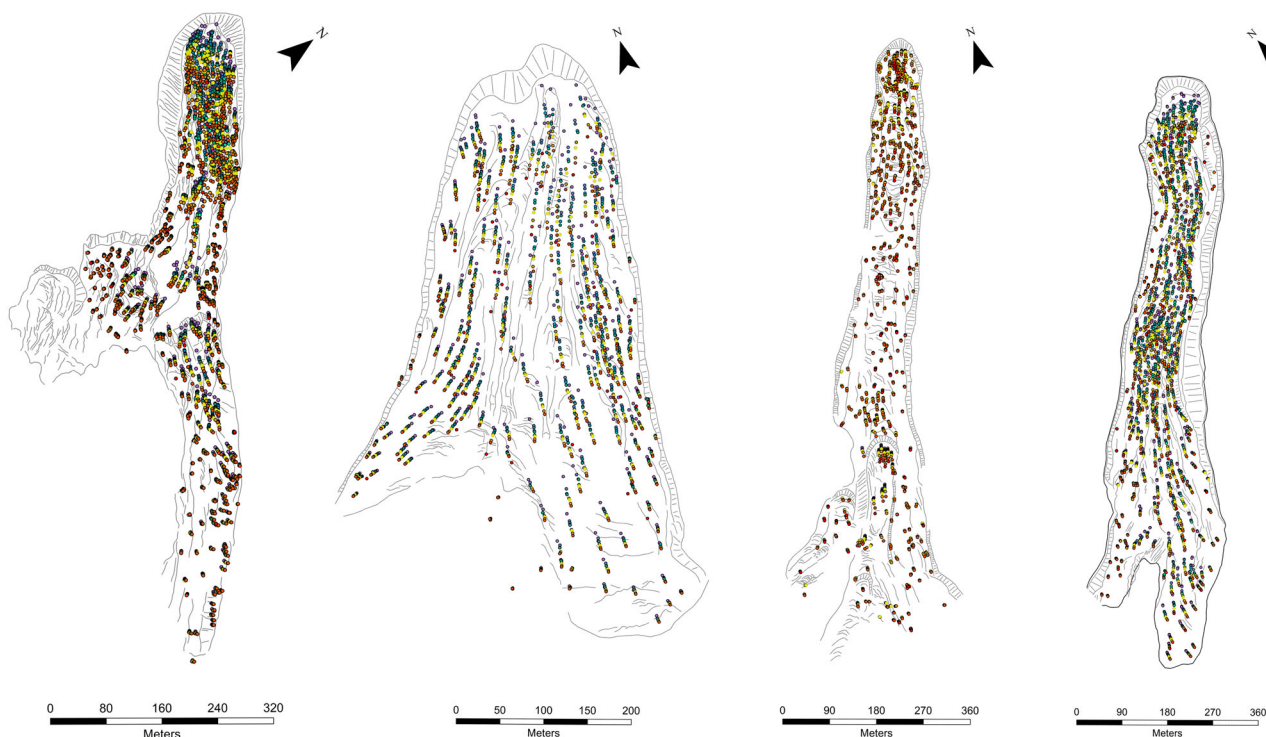
Historical aerial imagery (1946 to 2000). The Swisstopo[52] catalog presents a vast spatial and temporal coverage of historical aerial imagery. We have downloaded and pre-processed each of the available scanned historical images that cover our study area (651 images) for all the available dates, comprising 1946, 1956, 1962, 1973, 1979, 1985, 1988, 1991, 1997, 2000 and 2003. For some of the years, more than one acquisition date is available. When that befalls, we have always chosen a single date, being the one with the best resolution, greatest spatial overlap between datasets, and with less snow cover and/or shadowed areas.

To obtain better detail in the shaded areas, we have individually pre-processed each of the scanned images by adjusting brightness and contrast. Besides, if necessary, we have applied sharpening filters and matched levels between datasets that would be processed together. These adjustments considerably increase the final accuracy of the photogrammetry models, facilitate the pixel matching between datasets, and reduce the point cloud noise in the brighter and shaded areas. Despite these improvements, afterwards, manual cleaning of the point clouds noise for each of the photogrammetry models has been necessary.

Ground control points (GCP), used during the photogrammetry process, were acquired in different field campaigns with a Trimble Geo7x and post processed to obtain DGNSS locations from stable boulders, located in the immediate vicinity of the active areas of each RG (SD6). Stability of these boulders was assessed by measuring the relative distances in the historical imagery between the boulders and different close bedrock outcrops, against the relative distances in the most recent Swisstopo orthophoto from 2019[52]. Finally, just the locations with highest precision (vertical and horizontal accuracy o + −10 to + −40 cm) were selected as GCP candidates for the photogrammetry processing. For the more inaccessible upstream areas, GCP of stable outcrops were selected using XY coordinates from the 2019 Swisstopo orthophoto (10 cm pixel resolution) and Z values from the 2015 SwissALTI DEM (0.5 m)[69]. The horizontal and vertical accuracy of these upstream GCP is much lower $(+ - 2\,m)$ than the ones of the downstream DGNSS GCP. Even so, it is a sufficient precision for our purposes, since in these upstream areas we do not realize measurements of horizontal displacements and the elevation changes are normally greater than the measured uncertainty for each period.

Photogrammetry processing has been carried out using Pix4Dmapper 4.5.6 software separately for each RG and for each different date, resulting in 40 different orthophotos and 40 DSMs (10 for each RG) with pixel resolutions between 0.2 to 0.7 m. Unfortunately, it was not possible to obtain satisfactory models from 2003 due to lower levels of overlap in the imagery.

UAV in Val da l'Acqua (2022). After the aperture of new cracks exposing fresh ice in the Adjacent Glacier of Val da l'Acqua during 2022 summer of 2022, the GIS group of the SNP asked for a UAV survey in order to map the observed geomorphological changes. Hence, we carried out the

Fig. 8 | Locations of tracked boulders. Positions of the manually tracked boulders that have been used to calculate horizontal surface velocities for different periods between 1946–2022 for the four rock glaciers. The table below shows the tracked boulder densities and area (ha) of each rock glacier active area.

survey covering the entire Contributing Glacier and RG area during September 2022, using an Ebee RTK drone. Through the same photogrammetry procedure as used for the historical imagery, we created an orthophoto and a DSM with a resolution of 10 cm per pixel. In this case, the use of GCPs was not necessary, since the RTK gave a better average horizontal and vertical accuracy of $+ − 2$ cm for the entire area. These UAV orthophoto and DSM were used as reference for the co-registration of the rest of Val da l'Acqua photogrammetry models from the historical imagery.

Horizontal velocities assessment - Manual boulder tracking

Horizontal velocities were assessed by visual identification and tracking of boulders through consecutive images, using the orthophotos obtained from photogrammetry. As the upstream limit of the active areas are normally diffuse and may evolve over time, we tracked boulders up to the areas upstream where we do not identify any movement starting from the oldest period (1946–1956). With that, we have defined for each RG an active area limit within which we have evaluated the subsequent dynamic analyses.

The total number and density of point locations per rock glacier is dependent on the availability of boulders on the surface of each RG, trying to ensure that in each case there is a homogeneous spatial distribution, which is

necessary for a subsequent interpolation of the speeds for the entirety of the RG active areas. In total, for the four RGs analyzed, we have interpreted and manually digitized 12,000 different boulder locations along the different periods (Fig. 8).

Horizontal velocities for each period were calculated by computing the linear distance between XY coordinates of each tracked boulder at each date and dividing it by the number of years for the corresponding period, to obtain average surface displacements in cm a^{-1}. Finally, we created 1 m pixel resolution interpolated velocity maps for each period (Fig. 4) by Inverse Distance Weight (IDW) interpolation method, using the active RG limit as a boundary area with zero velocity value.

Elevation change – DSM differences

Elevation changes were calculated by means of DSM differences (DSM-d) to estimate cell by cell the change between the different DSMs. Computations were performed for the entire catchment area of each RG, in order to include both active RG areas and adjacent areas. Besides, DSM-d were only established for DSM datasets in which the upstream area does not show important snow cover and/or too much noise. For the most recent dataset we used the 0.5 m SwissALTI 2015 DSM from Swisstopo. Taking these criteria into account, the periods in which DSM-d have been computed are:

1956-1962-1973-1988-1991-1997-2015 for Tantermozza; 1956-1962-1973-1991-2015 for Valletta and Val Sassa; 1956-1973-1988-1991-2000-2015-2022 for Val da l'Acqua (Fig. 4, 5).

Despite the manual removal of the point cloud noise during the photogrammetry processing, final DSMs could still present wrong pixels that needed to be masked for the purpose of removing miscalculations in DSM-d. Noise masking areas were manually digitized by interpreting DSM hill-shades where these errors were easily identifiable (SD7). Finally, total elevation differences were divided by the number of years during each corresponding period to obtain elevation changes in cm a^{-1}.

Inferred adjacent glacier extensions
Adjacent Glaciers in our study area are currently covered by debris material, hiding partially (Tantermozza and Valletta) or completely (Val Sassa and Val da l'Acqua) their boundary limits. The debris cover layer has been evolving since 1946, when the total exposed ice area was much greater than in recent decades, creating challenges for mapping the historical presence of ice bodies. Here we infer the most probable historical glacier boundaries by assuming that ice presence must be related with the areas in which the highest elevation changes occur. Accordingly, big negative values in the DSM-d would correspond to periods with considerable ablation and important positive DSM-d values with accumulation periods

In a context in which the ablation is continuous for a total period of time, the longer the period considered, the greater the negative differences in the DSM-d values and, therefore, the limits in which this process occurs will be better spatially defined. Thus, we compute DSM-d between the different DSMs and the most recent DSMs (2015 for Tantermozza, Valletta and Val Sassa and 2022 for Val da l'Acqua). From these longer-period DSM-d maps, the limits of the total negative elevation difference, which would most likely correspond with the most probable ice melting area during the entire period, are clearly recognizable (SD2). We analyze these limits together with visual interpretation of geomorphological features in the corresponding orthophotos, to finally digitize the boundary of the most probable maximum ice extension on each date and infer it as the most probable Adjacent Glacier boundaries for each historical dataset. Furthermore, we compare our inferred extents with previously published historical extents in the Swiss Glacier Inventories of 1850 (SGI1850 from Dufour map), 1900, 1935 (Siegfried maps) and 1973 (SGI1973)[50,51,54,70].

Volume change calculations
For each time period, we have used the DSM-ds to individually determine the total volume change within active RG areas and inferred Adjacent Glacier boundaries. For simplification, we have only referred to the inferred area of the Adjacent Glaciers and not to the entire adjacent area, since in all cases the volume change in the inferred areas of the Adjacent Glacier corresponds to more than 95% of the total volume change of the adjacent area. Also, in Tantermozza we have not considered the marginal westernmost inferred glacier areas as it would not drain directly over the RG active area.

To compute total volumes from DSM-d where voids are present after the masking of the DSM noise areas, we use the *Mean elevation difference by elevation bin method*. This is a broadly used approach[71–73], which has proved accurate for mass balance calculations when using unfilled DEMs or DSMs[74,75]. This method involves firstly computing the DSM-ds using the voided DSM and binning the resulting raster in bigger grid cells with the mean values of the aggregated pixels. The choice of the bins (or grid cells) size depends on the total elevation range for the area considered. We follow McNabb's recommendations[74] of using a grid cell size equal to 10% of the elevation range in our analyzed area. This first step will fill the smaller voids in the DSM-ds. To fill the remaining voids, the binned raster is interpolated by a third order Local Polynomial interpolation. Finally, to obtain the volume per grid cell, the resulting mean elevation change binned raster needs to be multiplied by the area of each grid cell. The total volume for each

analyzed area consists of the total sum of the bin volumes within the boundary areas. (Supplementary Data 2).

Uncertainty assessment of photogrammetry measures
Even with the use of identical GCPs during the photogrammetric process, there may be important local distortions in the alignment of the generated orthophotos and DSMs. This translates into an imprecision in the co-registration of the images that must be taken into account as relative uncertainties in the horizontal and vertical measurements. The uncertainty should be considered as a threshold measure or level of detection (LoD)[76], above which we can begin to consider our displacement measurements as reliable. To quantify horizontal and vertical overall errors on each dataset comparison (Supplementary Data 9), we firstly create random points in mapped un-changed bedrock areas, which are as close as possible to the RG and the inferred Adjacent Glacier areas. Then, we register both vertical and horizontal differences of these random points for each image-pair and interpolate them (IDW), with the aim of avoiding spatial bias in the target areas. From this interpolated vertical and horizontal relative error maps we compute for each period the mean and standard deviation values within each rock glacier and Adjacent Glacier areas. Finally, the horizontal uncertainty can be considered as the mean values (*disp_xy*) plus 2 times the standard deviation (*dispσ_xy*) (95% confidence level) of the displacements (Eq. 1)[13].

$$error_{xy} = disp_{xy}(epoch1 - epoch2) + 2\,dispσ_{xy}(epoch1 - epoch2) \quad (1)$$

Meanwhile, the vertical error can be considered as 2 times the standard deviation of the DSM-d in the stable areas (*dispσ_z*)[16] and the volume uncertainty (*error_V*) for each Adjacent Glacier or RG area results from the multiplication of the vertical error by the corresponding area (Eq. 2)

$$error_V = \{2dispσ_z(epoch1 - epoch2)\}(area) \quad (2)$$

References
1. Reinosch, E. et al. Rock glacier inventory of the western nyainqêntanglha range, Tibetan plateau, supported by insar time series and automated classification. *Permafr. Periglac. Process.* **32**, 657–672 (2021).
2. Haeberli, W. & Burn, C. R. *Natural hazards in forests: Glacier and permafrost effects as related to climate change.* (CABI Publishing, Wallingford, 2002).
3. Hilario, A. et al. The First 100 Geological Heritage Sites. IUGS 60th anniversary report (ed. Hilario, A.) **1**, 242–243 (Int. Union Geol. Sci., 2022).
4. Chaix, A. Les coulées de blocs du Parc National suisse d'engadine (note préliminaire). *Le. Globe. Rev. Genev. de. Géographie* **62**, 1–35 (1923).
5. Capps, S. R. Rock glaciers in Alaska. *J. Geol.* **18**, 359–375 (1910).
6. Wahrhaftig, C. & Cox, A. Rock glaciers in the Alaska range'. *Geol. Soc. Am. Bull.* **70**, 383 (1959).
7. Chaix, A. Les coulées de blocs du Parc National Suisse. nouvelles mesures et comparaison avec les «rock stream» de la sierra nevada de californie. *Le. Globe. Rev. Genev. de. Géographie* **82**, 121–128 (1943).
8. Fleischer, F. et al. Combination of historical and modern data to decipher the geomorphic evolution of the Innere ölgruben Rock

Glacier, Kaunertal, Austria, over almost a century (1922–2021). *Permafr. Periglac. Process.* **34**, 3–21 (2022).

9. Kellerer-pirklbauer, A. & Kaufmann, V. About the relationship between rock glacier velocity and climate parameters in central Austria. *Austrian J. Earth Sci.* **105**, 94–112 (2012).

10. Tanarro, L. M. et al. Unchanged surface morphology in debris-covered glaciers and rock glaciers in Tröllaskagi Peninsula (northern Iceland)'. *Sci. Total Environ.* **648**, 218–235 (2019).

11. Cusicanqui, D. et al. Interpretation of volume and flux changes of the Laurichard Rock Glacier between 1952 and 2019, French Alps. *J. Geophys. Res.: Earth Surface* **126**, https://doi.org/10.1029/2021JF006287 (2021).

12. Kääb, A. et al. Inventory and changes of Rock Glacier creep speeds in Ile Alatau and Kungöy Ala-too, Northern Tien Shan, since the 1950s. *Cryosphere* **15**, 927–949 (2021).

13. Fleischer, F. et al. Multi-decadal (1953–2017) rock glacier kinematics analysed by high-resolution topographic data in the Upper Kaunertal, Austria. *Cryosphere* **15**, 5345–5369 (2021).

14. Marcer, M. et al. Rock glaciers throughout the French Alps accelerated and destabilised since 1990 as air temperatures increased. *Commun. Earth Environ.* **2**, 81 (2021).

15. Hartl, L. et al. Multi-sensor monitoring and data integration reveal cyclical destabilization of the äußeres Hochebenkar Rock Glacier. *Earth Surf. Dyn.* **11**, 117–147 (2023).

16. Fey, C. & Krainer, K. Analyses of UAV and GNSS based flow velocity variations of the Rock Glacier Lazaun (ötztal Alps, South Tyrol, Italy). *Geomorphology* **365**, 107261 (2020).

17. Bearzot, F. et al. Kinematics of an alpine rock glacier from multi-temporal UAV surveys and GNSS Data. *Geomorphology* **402**, 108116 (2022).

18. Brencher, G., Handwerger, A. L. & Munroe, J. S. Insar-based characterization of Rock Glacier Movement in the Uinta Mountains, Utah, USA. *Cryosphere* **15**, 4823–4844 (2021).

19. Bertone, A. et al. Incorporating insar kinematics into rock glacier inventories: Insights from 11 regions worldwide. *Cryosphere* **16**, 2769–2792 (2022).

20. Maurer, H. & Hauck, C. Geophysical imaging of Alpine Rock Glaciers. *J. Glaciol.* **53**, 110–120 (2007).

21. Kunz, J., Ullmann, T. & Kneisel, C. Internal structure and recent dynamics of a moraine complex in an Alpine Glacier Forefield revealed by Geophysical Surveying and sentinel-1 insar time series. *Geomorphology* **398**, 108052 (2022).

22. Arenson, L., Hoelzle, M. & Springman, S. Borehole deformation measurements and internal structure of some rock glaciers in Switzerland. *Permafr. Periglac. Process.* **13**, 117–135 (2002).

23. Buchli, T. et al. Kinematic investigations on the Furggwanghorn Rock Glacier, Switzerland. *Permafr. Periglac. Process.* **29**, 3–20 (2018).

24. Kenner, R., Pruessner, L., Beutel, J., Limpach, P. & Phillips, M. How rock glacier hydrology, deformation velocities and ground temperatures interact: Examples from the Swiss alps. *Permafr. Periglac. Process.* **31**, 3–14 (2019).

25. Kääb, A., Frauenfelder, R. & Roer, I. On the response of rockglacier creep to surface temperature increase. *Glob. Planet. Change* **56**, 172–187 (2007).

26. Delaloye, R., Lambiel, C. & Gärtner-Roer, I. Overview of rock glacier kinematics research in the Swiss alps. *Geographica Helvetica* **65**, 135–145 (2010).

27. Müller, J., Vieli, A. & Gärtner-Roer, I. Rock glaciers on the run – understanding rock glacier landform evolution and recent changes from Numerical Flow Modeling. *Cryosphere* **10**, 2865–2886 (2016).

28. Cicoira, A. et al. A general theory of Rock Glacier Creep based on in-situ and Remote Sensing Observations. *Permafr. Periglac. Process.* **32**, 139–153 (2020).

29. Roer, I. et al. Observations and considerations on destabilizing active rock glaciers in the European Alps. In *9th International Conference on Permafrost* 1505–1510 (2008).

30. Cicoira, A., Beutel, J., Faillettaz, J. & Vieli, A. Water controls the seasonal rhythm of Rock Glacier Flow. *Earth Planet. Sci. Lett.* **528**, 115844 (2019a).

31. Ikeda, A., Matsuoka, N. & Kääb, A. Fast deformation of perennially frozen debris in a warm rock glacier in the Swiss alps: An effect of liquid water', Journal of Geophysical Research: Earth Surface, 113, https://doi.org/10.1029/2007jf000859 (2008).

32. Cicoira, A., Beutel, J., Faillettaz, J., Gärtner-Roer, I. & Vieli, A. Resolving the influence of temperature forcing through heat conduction on Rock Glacier Dynamics: a numerical modelling approach. *Cryosphere* **13**, 927–942 (2019b).

33. Croce, F. A. & Milana, J. P. Internal structure and behaviour of a Rock Glacier in the arid Andes of Argentina. *Permafr. Periglac. Process.* **13**, 289–299 (2002).

34. Sommer, C. et al. Rapid glacier retreat and downwasting throughout the European Alps in the early 21st Century. *Nat Commun.* **11**, 3209 (2020).

35. Delaloye, R. et al. Rapidly moving rock glaciers in Mattertal. In C. Graf (Ed.), Mattertal – ein Tal in Bewegung p. 21-31. Eidg. Forschungsanstalt für Wald, Schnee und Landschaft WSL (2013).

36. Haeberli, W. In *Mitteilungen Der Versuchsanstalt Fur Wasserbau, Hydrologie Und Glaziologie* 5-142 (Eidgenossischen Technischen Hochschule, 1985).

37. Potter, N. Ice-cored Rock Glacier, Galena Creek, Northern Absaroka Mountains, Wyoming. *Geol. Soc. Am. Bull.* **83**, 3025 (1972).

38. Monnier, S., Camerlynck, C., Rejiba, F., Kinnard, C. & Galibert, P. Evidencing a large body of ice in a Rock Glacier, vanoise massif, northern French Alps. *Geografiska Annaler: Ser. A, Phys. Geogr.* **95**, 109–123 (2013).

39. Guglielmin, M., Ponti, S. & Forte, E. The origins of Antarctic Rock Glaciers: periglacial or glacial features? *Earth Surf. Process. Landf.* **43**, 1390–1402 (2018).

40. Berthling, I. Beyond confusion: rock glaciers as cryo-conditioned landforms. *Geomorphology* **131**, 98–106 (2011).

41. Ribolini, A. et al. The internal structure of rock glaciers and recently deglaciated slopes as revealed by Geoelectrical Tomography: Insights on permafrost and recent glacial evolution in the central and western alps (Italy–France). *Quat. Sci. Rev.* **29**, 507–521 (2010).

42. Dusik, J.-M. et al. Influence of glacier advance on the development of the multipart Riffeltal Rock Glacier, Central Austrian Alps. *Earth Surf. Process. Landf.* **40**, 965–980 (2015).

43. Monnier, S. & Kinnard, C. Reconsidering the glacier to rock glacier transformation problem: new insights from the Central Andes of Chile. *Geomorphology* **238**, 47–55 (2015).

44. Monnier, S. & Kinnard, C. Interrogating the time and processes of development of the Las Liebres Rock Glacier, Central Chilean Andes, using a numerical flow model. *Earth Surf. Process. Landf.* **41**, 1884–1893 (2016).

45. Sanjosé Blasco, J. J. et al. Geomatic techniques applied to the Dynamic Study (2001–2019) of the Rock Glacier in the Veleta Cirque (Sierra Nevada, Spain). *Land* **11**, 613 (2022).

46. Böhlert, R. et al. Application of a combination of dating techniques to reconstruct the Lateglacialand early Holocene landscape history ofthe Albula region (eastern Switzerland). *Geomorphology* **128**, 1–13 (2011).

47. Amschwand, D. et al. Deciphering the evolution of the bleis marscha rock glacier (val d'err, Eastern Switzerland) with cosmogenic nuclide exposure dating, aerial image correlation, and finite element modeling. *Cryosphere* **15**, 2057–2081 (2021).

48. Kenner, R. Geomorphological analysis on the interaction of alpine glaciers and rock glaciers since the Little Ice Age. *Land Degrad. Dev.* **30**, 580–591 (2018).

49. Palacios, D. et al. Reversible glacial-periglacial transition in response to climate changes and Paraglacial Dynamics: A case study from Héðinsdalsjökull (Northern Iceland). *Geomorphology* **388**, 107787 (2021).

50. Maisch, M. et al. *Die Gletscher der Schweizer Alpen: Gletscherhochstand 1850, Aktuelle Vergletscherung, Gletscherschwundszenarien. Schlussbericht NFP 31* 2nd edn (vdf Hochschulverlag ETH Zurich, 2000).

51. Müller, F., Caflisch, R. & Müller, G. Firn und Eis der Schweizer Alpen: Gletscherinventar. *Publ. Geographisches Institut, Eidgenössische Technische Hochschule* 57–57a (ETH, Geographisches Institut, Zürich, 1976).

52. Swissimage. Bundesamt für Landestopografie swisstopo (2023). Available at: https://www.swisstopo.admin.ch/de/geodata/images/ortho/swissimage10.html (Accessed: 7th August 2023).

53. Copernicus. C3s Climate Bulletin shows Summer 2022 was Europe's warmest on record. Home Available at: https://climate.copernicus.eu/c3s-climate-bulletin-shows-summer-2022-was-europes-warmest-record (Accessed: 7th August 2023).

54. Freudiger, D. et al. Historical glacier outlines from digitized topographic maps of the Swiss alps. *Earth Syst. Sci. Data* **10**, 805–814 (2018).

55. Lambiel, C. & Reynard, E. Regional modelling of present, past and future potential distribution of discontinuous permafrost based on a Rock Glacier Inventory in the Bagnes-Hérémence Area (western Swiss alps). *Nor. Geografisk Tidsskr. - Nor. J. Geogr.* **55**, 219–223 (2001).

56. Seppi et al. Inventory, distribution and topographic features of rock glaciers in the southern region of the Eastern Italian alps (Trentino). *Gegr. Fis. Dinam. Quat.* **35**, 185–197 (2012).

57. Wagner, T. et al. The first consistent inventory of rock glaciers and their hydrological catchments of the Austrian alps. *Austrian J. Earth Sci.* **113**, 1–23 (2020).

58. Boeckli, L., Brenning, A., Gruber, S. & Noetzli, J. Permafrost distribution in the European alps: calculation and evaluation of an index map and summary statistics. *Cryosphere* **6**, 807–820 (2012).

59. Springman, S. M. et al. Rock Glacier degradation and instabilities in the European Alps: A characterisation and monitoring experiment in the Turtmanntal, CH. *Landslide Sci. Practi.* 5–13, https://doi.org/10.1007/978-3-642-31337-0_1 (2013).

60. Luetschg, M. & Haeberli, W. Permafrost evolution in the Swiss alps in a changing climate and the role of the snow cover. *Nor. Geografisk Tidsskr. - Nor. J. Geogr.* **59**, 78–83 (2005).

61. Barry, R. G. & Chorley, R. J. *Atmosphere, Weather and Climate* 9th edn (Routledge, 2010).

62. Jones, D. B., Harrison, S., Anderson, K. & Whalley, W. B. Rock glaciers and mountain hydrology: a review. *Earth-Sci. Rev.* **193**, 66–90 (2019).

63. Wuebbles, D. J. et al. Executive summary. climate science special report: Fourth national climate assessment, volume I. https://doi.org/10.7930/j0dj5ctg (2017).

64. Allen, M. R. et al. In *Global Warming of 1.5°C. An IPCC Special Report on the Impacts of Global Warming of 1.5°C Above Pre-industrial Levels and Related Global Greenhouse Gas Emission Pathways, in the Context of Strengthening the Global Response to the Threat of Climate Change, Sustainable Development, and Efforts to Eradicate Poverty* 49–92 (Cambridge University Press, 2018).

65. Waller, R. I. Permafrost and periglacial features | permafrost and Glacier Interactions. Encyclopedia Quater. Sci. 507–513. https://doi.org/10.1016/b978-0-444-53643-3.00107-2 (2013).

66. Sippel, S. et al. Late 1980s abrupt cold season temperature change in Europe consistent with circulation variability and long-term warming. *Environ. Res. Lett.* **15**, 094056 (2020).

67. Wirz, V. et al. Short-term velocity variations at three rock glaciers and their relationship with meteorological & nbsp; conditions'. *Earth Surf. Dyn.* **4**, 103–123 (2016).

68. Jäckli, H. Der blockstrom in der val da l'acqua im Schweizerischen Nationalpark. Jahrbuch der Schweizerischen Naturforschenden Gesellschaft. *Annu. Soc. Helv. Sci. Nat.* **158**, 213–221 (1978).

69. SwissALTI3D. Federal Office of Topography swisstopo (2023). Available at: https://www.swisstopo.admin.ch/en/geodata/height/alti3d.html (Accessed: 7th August 2023).

70. Linsbauer, et al. The new Swiss Glacier Inventory SGI2016: From a topographical to a glaciological dataset. Front. *Earth Sci*. 22, https://doi.org/10.3389/feart.2021.704189 (2020).

71. Kronenberg, M. et al. Mass-balance reconstruction for Glacier No. 354, Tien Shan, from 2003 to 2014. *Ann. Glaciol.* **57**, 92–102 (2016).

72. Brun, F., Berthier, E., Wagnon, P., Kääb, A. & Treichler, D. A spatially resolved estimate of High Mountain Asia Glacier Mass balances from 2000 to 2016. *Nat. Geosci.* **10**, 668–673 (2017).

73. Dussaillant, I., Berthier, E. & Brun, F. Geodetic mass balance of the northern Patagonian Icefield from 2000 to 2012 using two independent methods. *Front. Earth Sci.* **6**, 8 (2018).

74. McNabb, R. et al. Sensitivity of glacier volume change estimation to Dem Void Interpolation. *Cryosphere* **13**, 895–910 (2019).

75. Huber, J., McNabb, R. and Zemp, M. Elevation changes of west-central Greenland glaciers from 1985 to 2012 from Remote Sensing', *Front. Earth Sci.* 8, https://doi.org/10.3389/feart.2020.00035 (2020).

76. Vivero, S., Hendrickx, H., Frankl, A., Delaloye, R. & Lambiel, C. Kinematics and geomorphological changes of a destabilising rock glacier captured from close-range sensing techniques (Tsarmine rock glacier, Western Swiss Alps). *Front. Earth Sci*. **10**, 1017949 (2022).

Author contributions

A.M.T.M. compiled all the historical data, performed photogrammetric analysis and performed the vertical and horizontal measurements. S.A. M.S., A.C and A.M.T.M. designed the study. M.S. obtained the funding. S.W. and R.H. provided the database of historical (Chaix) and recent measurements (GNSS) and participated in field acquisition data together with A.M.T.M and M.S. All authors contributed in discussing and revising the analysis and findings.

Competing interests

The authors declare no competing interests.

Additional information